Final Report

p-58

NASA DRYDEN-PRC SYSTEM SERVICES
Flight Research Facility
Building No. 4839
Edwards, CA 93523-5000

Electro Optical System to Measure Strains at High Temperature

NASA-AMES Grant No. NAG2-547
7/16/90 - 12/31/91

By

Cesar A. Sciammarella
Illinois Institute of Technology
Department of Mechanical and Aerospace Engineering
Chicago, IL 60616

[1]NASA Technical Officer for this grant is: Lawrence F. Reardon, Ames Research Center, P.O. Box 273, Edwards, CA 93523-5000

TABLE OF CONTENTS

LIST OF TABLES

LIST OF FIGURES

INTRODUCTION

The measurement of strains at high temperatures has become a very important field of research. Advanced technology applications such as structures for high speed aircraft, high efficiency thermal engines, are examples of areas requiring measurements of strains at temperatures well above capability of the the present strain gage technology. In a recent paper by one of the authors[1] references on the application of optical techniques to field measurement of strains at high temperatures are given. Of the different techniques that are used, speckle and holographic interferometry are of particular interest. Both techniques are remote sensing and do not require elaborate preparation of the surfaces being investigated. From the view of practical applications the use of TV cameras for recording purposes and electro-optical data manipulation and processing are of great interest. Simplicity in handling the recording process, speedy data collection and automatic data processing are main advantages of using electro-optical methods. Some more developments in this field can be found in[2] to [6]. Reference[4] contains quantitative results proving the feasibility of making accurate measurements at temperatures up to 1000°C.

RESEARCH PROGRAM: ELECTRO-OPTICAL SYSTEM TO MEASURE STRAINS AT HIGH TEMPERATURES

The originally proposed program consisted of three different phases. Each of these phases had partial goals and objectives contributing to the final goal of developing the necessary technologies leading to a portable instrument capable of operating under field conditions.

The goal of the Phase-1 of the project was to demonstrate the feasibility of putting together an electro-optical device capable of performing strain measurements up to 2000°F.

The goal of Phase-2 of the project was to produce a first version of a portable system and to test it under field conditions.

The goal of the third Phase was to produce a prototype to suit NASA requirements.

The program started in 9/01/88 and was funded until 8/30/91.

Each Phase was divided into different tasks. The Research Tasks were devoted to the development of the necessary scientific basis to achieve the goal of the project. The Design and Construction Tasks were devoted to the following fundamental objectives: a) design and construction of the auxiliary equipment necessary to carry out the research; b) design and construction of the electro-optical system to measure strains; c) design and development of the necessary drivers and software to operate the hardware. The Testing Tasks were directed to perform high

temperature strain measurements. Finally, the Evaluation Tasks provided an analysis of the achievements of the program.

In the semi-annual reports we have provided the details of the achievements in the different tasks of the program. In this Final Report, particular emphasis will be put on the results of the high temperature tests. In what follows we will give a brief summary of the overall accomplishments of the program.

In the research aspect of the program, all the fundamental variables that control the measurement, recording and data processing of strains at high temperature were individualized and investigated.

A high temperature oven was designed and manufactured. Two different versions were developed, one with three windows and another with five windows.

Two different loading frames were designed and built.

Several versions of the electro-optical system to gather strain information were designed and built. Some components were assembled by integrating commercially available components. Other components were designed and built in our laboratory.

A large number of programs were developed to operate the system and to carry out other specialized tasks needed for data gathering and data processing.

In what follows we will provide a description of the electro-optical system as it stands currently.

PORTABLE ELECTRO-OPTICAL HOLOGRAPHIC INTERFEROMETER

To apply optical technology to the field of high temperatures, the system schematically shown in Fig. 1 has been designed. The system contains optical and electronic components that perform different functions; the guiding principle in the design of the instrument is to use each technology to its fullest advantage. From the systems point of view, one can distinguish the following components,

1) Illumination and light conditioning
2) Signal reception
3) Signal detection
4) Data processing
5) Data output
6) Host processor

The illumination system contains two subsystems, 1) fringe stabilization, 2) fringe shifting.

The signal reception is performed by a CCD camera. The detection and conditioning functions rest on several electronic components:

a) Analog to Digital and Digital to Analog Converter. This unit coverts the analog input coming from the CCD camera to digital form and the output of the system from digital to analog.
b) Arithmetic-logical Unit. This unit performs arithmetic and logical operations on the incoming signal.
c) Storage Memories or Frame Buffers. Several units store information during the processing operations.
d) Array Processor. A Parallel processor that performs certain operations with high efficiency resulting in considerable reduction in computing time.
e) Host Processor. The host processor controls the different components and performs some of the tasks in data processing.

The output of the system can be a graphic display that goes to a monitor or to a printer, or numerical values.

The input to the system is an image, from which the system can produce interference fringes that cover the observed surface. The output can be: displacements, strains, stresses, or contours of a surface. In the current configuration images can be recorded as a function of time within the speeds that can be handled by the American Standard Television System. High speed images can be recorded one at time, periodic phenomena can be observed by time average procedures or by stroboscopic techniques.

The fringe stabilization system enables the interferometer to operate without mechanical isolation. This system compensates rigid body motions, fiber optics instabilities and random fluctuations caused by air motion. This circuit has two main components: a) an opto-electric device with a piezo-electric phase shifter (PPS); b) an electronic circuit that provides the PPS with a voltage that compensates the phase changes due to the above mentioned causes. A light sensor, senses the light intensity of a small region of the body. This sensor receives the same information that the camera receives, except that it does it dynamically. This signal goes to a circuit where it is processed. Out of the circuit comes an error signal that is fed to the PPS.

One of the problems that affects the practical use of holographic interferometry is the loss of correlation caused by the rigid motions introduced by the application of load on the body that is analyzed. To take care of this problem the camera is supported on an universal motion system. This system receives a feedback signal from the imaging system. The feedback signal keeps the image fixed with respect to a reference system attached to the camera.

Both features of the interferometer have been implemented and tested at room temperature with satisfactory results.

ELECTRONIC HOLOGRAPHY

Electronic holography is referred in the literature as electronic speckle pattern interferometry (ESPI); extensive references can be found in[7]. Electronic holography can be classified as focused image holography. It obeys the classical equation of holographic interferometry,

$$n\lambda = \mathbf{d}\cdot\mathbf{S} \tag{1}$$

where n is the fringe order, λ is the wavelength of light, $\mathbf{d}$ is the displacement vector and $\mathbf{S}$ is the sensitivity vector. The fringes provide the displacements of the points of the observed surface projected on the sensitivity vector. In the recording process the main difference with ordinary holography is the low spatial resolution of the recording medium, when compared to film or light sensitive plastics. The low sensitivity makes it necessary to use a small angle between the reference and the observation beams. There is however, one main difference between the two types of holography; the image reconstruction process. The image reconstruction in electronic holography is performed by either electronic or digital techniques. To generate interference patterns, there are a number of alternative procedures; the traditional way[7] is image subtraction, a different procedure is used in[8]. To obtain quantitative data[9] provides another alternative. Whatever is the method used to produce fringe patterns, the signal has the form,

$$I(x,y) = I_0(x,y) + I_1(x,y)\cos\left[\phi(x,y) + \Delta\phi(x,y) + \alpha\right] \tag{2}$$

where I (x,y) is the intensity distribution on the surface subjected to analysis, $I_0(x,y)$ is a random background term, $I_1(x,y)$ is a random amplitude of the fundamental harmonic, $\phi(x,y)$ is a random variable phase, $\Delta\phi(x,y)$ is the change of phase produced by the applied loading and α is an initial phase that depends on the chosen coordinate system. The objective of our analysis is to obtain $\Delta\phi(x,y)$ or its rate of change.

DATA PROCESSING

Numerous schemes of data processing were developed and tried during the period of the research program. In what follows, we will describe the current state of software developed for data processing.

Computer assisted methods to retrieve fringe information where introduced by one of the authors[9]. The latest version with a number of improvements introduced on the original procedures can be found in[10]. In the past, due to the lack of low cost high speed hardware, operations where performed in one dimension. Recent improvements in the available hardware, have made it possible to implement 2-D techniques of fringe analysis. The developed techniques can be implemented either in the actual physical space or in the Fourier space. The choice of one or the other alternative depends on the total computational time. The Fourier space techniques require an initial Fourier transform and a final inversion; this additional operation can be compensated only if the total number of operations in the Fourier space is reduced when compared to processing in the physical space. The time balance depends on the number of terms used in the filtering of the data. When operating in 2-D, the problem of implementing an efficient filtering operation becomes critical and there is a definite time advantage to operate in the Fourier space. The method described in this paper applies in general to any fringe system. However in this report, we will discuss a version that applies to the holographic moire technique. In this technique[10] to [15], by using double beam illumination in two orthogonal directions, the displacement vectors are projected onto a reference plane.

The first operation is to perform a Fourier transform of the data,

$$FT[I(x,y)] = \bar{I}(\omega_1,\omega_2) \tag{3}$$

where the bar indicates the Fourier transform of the corresponding function, ω_1 and ω_2 are angular frequencies. The second operation is a filtering operation. The filters used are elliptical filters with smooth transitions,

$$\bar{I}^{*}(\omega_1,\omega_2) = \bar{I}(\omega_1,\omega_2)H(\omega_1,\omega_2) \tag{4}$$

where the * indicates the filtered version of the Fourier transform of the signal and the $H(\omega_1,\omega_2)$ are the filter weights. Taking the inverse Fourier transform,

$$F^{-1}[\bar{I}^{*}(\omega_1,\omega_2)] = I_1 \cos\Delta\phi_x = I_p \tag{5}$$

we get a signal that we call in-phase signal, that contains the phase information only, since the background term as well as the noise outside the bandwidth of the signal have been removed by the filter. To get the phase and the signal amplitude, the in-quadrature signal processing[10] is applied. The fast Fourier transform program that has been implemented, performs FFT of real functions only. To obtain the Fourier transform of the signal in-quadrature, the following operation is performed,

$$-j\,\mathrm{sgn}(\omega_1)\,\bar{I}^{*}(\omega_1,\omega_2) = \bar{I}_q^{*}(\omega_1,\omega_2) \tag{6}$$

where sgn indicates the signum function. One should notice that the signum function contains the variable ω_1, since one is interested in the projection of the vector displacement along the reference axes of the coordinate system, which in the case of equation (6) is assumed to be the x-axis. By taking the inverse of (6) one obtains the in-quadrature signal,

$$F^{-1}\left[\bar{I}_q^{*}(x_1,x_2)\right] = I_1 \sin\Delta\phi_x = I_q \tag{7}$$

The change of phase is computed using,

$$\Delta\phi_x(x,y) = \mathrm{arc\,tg}\frac{I_q}{I_p} \tag{8}$$

The phase information is obtained in the interval $-\pi$ to π and the continuity of the phase information is restored by a subroutine[10].

The amplitude is obtained by,

$$I_1 = \sqrt{I_p^2 + I_q^2} \tag{9}$$

and the fringe pattern can be normalized.

From the normalized pattern the derivatives of the pattern can be obtained by differentiation in the Fourier plane,

$$\bar{I}^{*}_{pn}(\omega_1,\omega_2)\, H_D[-j\omega_1] = \bar{I}'_{n}(\omega_1,\omega_2) \tag{10}$$

where the subscript, n, indicates the normalized spectrum and, ′, indicates the derivative, and

$$\bar{I}^{*}_{qn}(\omega_1,\omega_2)H_D(-j\omega_1) = \bar{I}'_{qn}(\omega_1,\omega_2) \tag{11}$$

By Fourier inversion,

$$F^{-1}[\bar{I}'_{pn}(\omega_1,\omega_2)] = \frac{\partial I_{pn}(x,y)}{\partial x} \tag{12}$$

and

$$F^{-1}[\bar{I}'_{qn}(\omega_1,\omega_2)] = \frac{\partial I_{qn}(x,y)}{\partial x} \tag{13}$$

and from these two components one obtains

$$\frac{\partial \Delta\phi_x(x,y)}{\partial x} = \left[\left(\frac{\partial I_{pn}}{\partial x}\right)^2 + \left(\frac{\partial I_{qn}}{\partial x}\right)^2\right]^{1/2} \tag{14}$$

Similar operation can be performed in the y-direction to obtain the cross derivative. By analyzing the pattern in the orthogonal direction, the other two derivatives can be obtained. Finally,

$$\epsilon_x = p\frac{\partial \Delta\phi_x}{\partial x} \tag{15}$$

$$\epsilon_y = p\frac{\partial \Delta\phi_y}{\partial y} \tag{16}$$

$$\epsilon_{xy} = \frac{1}{2}p\left(\frac{\partial \Delta\phi_x}{\partial y} + \frac{\partial \Delta\phi_y}{\partial x}\right) \tag{17}$$

where ϵ_x, ϵ_y and ϵ_{xy} are the components of the strain tensor, and $p = \frac{\lambda}{2 \sin \alpha}$, where α is the angle of illumination. If the surface is not a plane surface, the obtained strains must be reduced to the local coordinate system[16] and [17].

RECORDING OF HOLOGRAMS AT HIGH TEMPERATURE

The displacement information is encoded in the intensity modulation of the speckles[18] and the resulting fringe visibility is a function of the speckle visibility. If the object beam amplitude is given by,

$$E_o(r) = E_o(r)e^{i\phi_o(r)} \tag{18}$$

where $E_o(r)$ and $\phi_o(r)$ indicate the amplitude and phase of the points of the object as a function of the spherical coordinates, r, in the object space. When the surface of the object is rough, a speckle pattern appears at the image plane of the optical observation system. The intensity distribution is given by,

$$I(r') = \int\int k(r_1, r')\, k^*(r_2, r')\, \Gamma(r_1, r_2) \cdot$$

$$E_o(r_1)E_o(r_2)e^{i\left[\phi_o(r_1)-\phi(r_2)\right]}dr_1 dr_2 \tag{19}$$

where r' are the spherical coordinates in the image plane, k(r,r') is the spreading function of the imaging system, and $\Gamma(r_1,r_2)$ is the mutual coherence function of the illumination over the object. Equation (19) indicates that the image intensity

distribution depends on the spread function of the lens system, the random phase variations of the object and on the mutual coherence function.

Introducing the normalized standard deviation of the speckle intensity variations,

$$V = \frac{\left[< I^2(r') > - < I(r') >^2 \right]^{1/2}}{< I(r') >} \qquad (20)$$

where the brackets <...> indicate the ensemble average. Replacing (19) in (20) and introducing some additional assumptions[19] and [20], it is possible to conclude that the fringe visibility depends:

a) On the mutual coherence function
b) On the spread function $k(r_1,r_2)$ of the optical system
c) On the object surface roughness through the autocorrelation function of the phases $<\phi(r_m)\ \phi(r_n)>$ which in turn is a function of the rms roughness of the surface.

From[19] and [20], one can conclude that for each surface roughness there is an optimum aperture of the lens system that gives the best speckle visibility.

The mutual coherence function is affected by many factors. At high temperatures one of the main factors is the intensity radiated by the object in the wavelength of the laser used.

To understand the problems that arise when one attempts to record fringe patterns at elevated temperatures, it is necessary to look at the emissive power of hot surfaces. According to Kirchhoff's law the energy irradiated at a given wavelength does not depend on the particular substance involved but depends on its absolute temperature. Kirchhoff's law applies to a black body; in real materials the energy radiated depends on the emissivity of the surface, which is a function of the substance, the temperature, the wavelength, the state of the surface and the direction in the space. In metals, one can take as a first approximation the spectral distribution corresponding to the black body and use an emissivity coefficient smaller than one. The spectrum radiated by the black body can be found by applying Plank's equation.

The energy irradiated by the surface increases the average or background intensity and reduces the fringe visibility as defined by (20). The problem can be analyzed as a function of the wavelength of the laser light utilized to record the pattern and the power of the laser. To improve the fringe visibility, it is necessary to introduce a filter corresponding to the wavelength of the laser light utilized to illuminate the specimen. Filters have a spectrum that has the maximum

transmissibility at the peak value. An approximated calculation of the contrast loss that can be expected can be performed in the following way. The energy emitted the black body for a given temperature and a given wavelength can be obtained from tables[21]. The tables provide the value

$$E_{o\lambda} = \int_{o}^{\lambda} E_b \, d\lambda \tag{21}$$

where E_b is the energy at a given wavelength and a given temperature, and $E_{o\lambda}$ is the total energy up to the corresponding wavelength. If we introduce the bandwidth of the filter $\Delta\lambda$

$$E_{o\lambda_1} = \int_{o}^{\lambda_o - \Delta\lambda/2} E_b \, d\lambda \tag{22}$$

and

$$E_{o\lambda_2} = \int_{o}^{\lambda_o + \Delta\lambda/2} E_b \, d\lambda \tag{23}$$

the energy in the bandwidth is given by the difference between (22) and (23).

$$\Delta E = E_{o\lambda_2} - E_{o\lambda_1} \tag{24}$$

Figure 2 gives a graph of the energy emitted by the black body for λ = 514.5 nm and λ = 632.8 nm, for a bandwidth of 10 nm.

The loss of visibility due to the light intensity generated by the high temperature can be summarized as a ratio,

$$R = \frac{E_s c_r}{\Delta E \, c_e} \tag{25}$$

where E_s is the energy density of the illumination beam on the surface of the observed object, c_r is the coefficient of reflectivity of the surface, ΔE is the energy density irradiated by the surface in the bandwidth of the filter used to remove unwanted illumination from the observation system, and c_e is the emissivity of the surface. To increase the fringe visibility it is necessary to make R as high as possible. We can see from Fig. 2 that, by going to shorter wavelengths, one can reduce ΔE. One should make E_s as high as possible. The coefficient of reflectivity can be improved by putting a reflective coating capable of withstanding the temperature. One can reduce the bandwidth of the filter but this change affects also E_s, since the transmissibility of the filter is also reduced when the bandwidth is reduced.

Two other factors affect the speckle visibility, a) mechanical vibrations of the object, the illumination sources and of other components of the optical system, b) changes of optical phase caused by air density variations produced by thermal convective currents. Both effects can be reduced by reducing the exposure times using cameras that have a shutter. Of course time exposure reduction if it is not compensated by increased light intensity, in turn, causes a deterioration of the signal.

To the above causes of visibility loss, we have to add effects that change the correlation between the initial or reference image and the subsequent images compared with the reference image. The fringe visibility[14] is a function of the decorrelation of the two compared images. The main variable[14] controlling the visibility is the ratio of the displacement of the points due to the loading to the speckle size. In[14] it is shown that fringe visibility due to rigid body motions can be compensated by moving the recording device until maximum visibility is observed. Another important effect is the changes of the surface due to temperature, such as oxidation. This factor may limit the time that can be used to observe fringe patterns.

So for, we have discussed the effect of the high temperature on the fringe visibility. Another effect of the temperature is to introduce random phase components to the fringe patterns.

If we consider the propagation of a light beam through the airs taking place in the z-direction, the phase change recorded by a double exposure hologram is

$$\Delta\phi(x,y) = \int_{o}^{z_i} [n(x,y,z) - n_o(x,y,z)] dz \tag{26}$$

where $n_o(x,y,z)$ is the index of refraction at the time of the initial recording and $n(x,y,z)$ is the index of refraction at the second exposure. The index of refraction of a gas is given by the equation,

$$n = 1 + K\frac{mp}{RT} \tag{27}$$

K is a constant, which is a function of the wavelength of light and the type of gas, m is the molecular weight, p is the pressure, R is the universal gas constant, and T is the absolute temperature. The turbulent motion caused by convective currents in the neighborhood of the heated body produces random changes in the density, the pressure and temperature. These changes result in random phases which are added to the changes of phase caused by the loading. These changes of phase will not be eliminated by using high speed recording. If we are dealing with static or low speed loadings the changes of phase produced by the loading are stationary in time and space while the changes of phase caused by the thermal effect are random in space and time.

TEST TO INVESTIGATE THE EFFECT OF THE APERTURE OF THE RECORDING CAMERA

The first series of tests were devoted to investigate the effect of the aperture of the recording camera.

Figure 3 shows the utilized optical set-up. Two rectangular bars were used as models. The bars were inside an oven. The front window could be closed with a high temperature silica window. Observations were made with and without the window. The test showed that, from the point of view of the patterns, there was not much difference between operating with or without the window. The measurements were carried out with the window to minimize the heat loss.

The furnace has a thermocouple that displays its temperature; the temperature was measured also by another thermocouple fixed to the specimens and recorded by a digital thermometer with the accuracy of 1°F.

The object was illuminated by a double beam illumination; the corresponding sensitivity of the system was 0.9251 microns per fringe. In one of the illumination beams, there was a mirror that could be rotated to generate carrier fringes. The laser used for illumination was a helium-neon laser operating at 632.8 nm wavelength and at a power of 50 mW.

An interference filter was introduced in front of the lens of the CCD camera. The filter is rated for maximum transmission of 56.8% at 632.8 nm wavelength. The

bandwidth of the filter, defined as the band measured between points where the transmission has fallen to one half of the maximum, is 3.5 nm.

Two specimens were investigated; a ceramic specimen - a Norton silicon carbide bar and a Haynes alloy No. 230. The Haynes alloy is a nickel-cromium-tungsten-molybdenum alloy which has good high-temperature strength and a resistance to oxidation up to 1,150°C.

During the tests, the SiC bar did not change the appearance of the surface; it remained shiny and smooth. The Haynes alloy became covered by a black oxide; in view of this phenomenon, all the experiments for the Haynes alloy were performed in the oxidized condition.

A series of experiments were carried out to define the main characteristics of the optical parameters that influence the fringe contrast at high temperatures. The coefficient of expansion of the Haynes alloy 230 was measured between 797°C to 986°C.

In Fig. 4 the image intensity measured after the filter is plotted as a function of the image intensity before the filter for apertures 1/9, 1/12, 1/14 and 1/16 of the lens system and an illumination intensity in the object plane of 0.20 mW/cm^2. The filter is rated as having a transmission coefficient of 58.6% at 632.8 nm; Fig. 4 gives a transmission coefficient of 46.7%. This quantity agrees well with the data provided for the filter, at 46.7% transmission the bandwidth is 2.5 nm.

Tables I and II summarize some of the quantities measured in the tests. Of particular significance are the ratio C, ratio between the illumination received by the object and the intensity generated by the temperature. For the SiC bar, this ratio is 16.6% and 16.9% for the Haynes alloy in the oxidized condition. This ratio must be compared with the ratio J of intensities after the filter in the image plane. This quantity for the SiC bar is 33.3% and indicates that the filter has been very effective in reducing the effect of the energy emitted by the heated surface. For the Haynes alloy, J is only 7.3%, this reduction is caused by the dropping of the amount of the light returned by the oxidized surface of the alloy.

Figure 5 shows the intensity in the image plane after the filter as a function of the lens aperture for the SiC bar (room temperature). If the illumination was uniform, this function should change with the ratio of the square of the radii of the apertures, however since the illumination is stronger at the center than at the periphery of the aperture, the actual function although quadratic shows lesser reduction of the intensity than the ratio of the squares of the radii. Figure 6 shows the experimentally determined fringe visibility in the monitor screen versus the speckle radius for the SiC ceramic bar. The fringe patterns were generated by rotating one of the illumination beams, in all cases the amount of rotation was the same. The speckle radius is computed by means of the equation:

$$\rho = \frac{0.61\pi}{NA} \tag{28}$$

where NA is the numerical aperture of the lens system. All the patterns are recorded with the same electronic gain. There are two room temperature curves, one without window, the other with a window. The presence of the window reduces the visibility, as one could expect, since some amount of light will be reflected by the window. The high temperature curve corresponds to 1000°C; the patterns were recorded with a window. As shown in[19] and[20] there is an optimum numerical aperture that yields maximum visibility. The plot in Fig. 6 shows a steeper loss of visibility with increasing speckle size than the curves shown in[19] and[20].

Figure 7 shows for the SiC bar the relation between the intensity at the image plane after the filter at high temperature (1000°C) versus the same intensity at room temperature. The measurements were carried out for the aperture 1/9. The high temperature values were determined by subtracting from the intensities at high temperature with laser illumination, the intensities without illumination. The slope of the resulting line is approximately one, indicating that for the ceramic bar the reflectivity remains almost constant from room temperature to 1000°C.

Figure 8 shows for the Haynes 230 alloy, the fringe visibility as a function of the speckle radius at room temperature for the fully oxidized surface. The lower points correspond to visibilities measured for the 1/7 aperture at the indicated temperatures. The electronic gains were not kept constant for the high temperature due to the fact that the average intensity saturated the camera, thus the gains have to be reduced with the increasing temperature.

Figure 9 shows the measurement of the coefficient of expansion of the Haynes alloy as a function of the temperature between 797 and 986°C. The measurements were carried out by introducing a system of carrier fringes and recording the changes of the carriers for intervals of temperature ranging from 5°F to 10°F, depending from the visually observed deterioration of the fringe visibility with displacement and time. Although they are not exactly comparable, data provided by the manufacturer are also plotted. These coefficients are averages from room temperature to the high temperature. Both curves show the same trend and there is also a numerical agreement. The coefficient of expansion between 25-100°C is 12.7 x 10^{-6} °C and between 25-1000°C is 16.1 x 10^{-6} °C. If we average the 12.7 with the 18.5 at 1000°C, computed from the second order polynomial that fits all the measured points, we get 15.6 which is only 3.1% from the value 16.1 given by the manufacturer for the average between 0 to 1000°C, and excellent agreement. The actually measured strains used to plot the coefficient of expansion curve ranged from 50.4 x 10^{-6} at 986°C to 97.3 x 10^{-6} at 836°C.

DISCUSSION AND CONCLUSIONS CONCERNING THE FIRST SERIES OF HIGH TEMPERATURE TESTS

The first series of test was devoted to the study of the main variables controlling the fringe visibility. The effect of the aperture on fringe visibility confirmed the theory presented in[19] and[20].

The measurements performed in the oxidized Haynes alloy show that even at very low light intensities (only 7.3% of the background light) one can perform very accurate measurements at 1000°C. The light intensity was .2 mW/cm^2. The conclusion is that one can perform accurate measurements at 1000°C even in poorly reflecting surfaces.

Two improvements were suggested by this series of tests. One is to cover the surface to be analyzed with a light reflecting ceramic. A filter with a reduced bandwidth is another possibility to improve the ratio R defined by equation (25).

Assuming a 80% effective delivery, with a 1.5 watts of coherent light at 531.4 nm wavelength, an argon-ion laser could provide illumination for about a square meter. In this calculation, a .2 mW/cm^2 light intensity density and the improvement resulting from a shorter wavelength were used.

SECOND SERIES OF TESTS

The first series of tests provided information concerning the variables controlling fringe visibility. This series also proved the feasibility of accurate strain measurements at 1000°C. A second series of tests was programmed. A disk under diametrical compression was chosen as a model. To perform the tests, a high temperature oven and a loading frame were designed and built. Figure 10 shows the cross section of the oven and the corresponding loading frame. Figure 11 shows the detail of the oven door. The door has three windows, a central window to view the model and two lateral windows for illumination at 45°. To insure the stability of the loading, the load was applied through a silicon carbide rod guided by a lateral bearing. The specimen was supported by another silicon carbide rod. The specimen was instrumented with thermocouples and with high and low temperature strain gages. The location of the thermocouples and strain gages is shown in Fig. 12.

Preliminary tests provided valuable information concerning two important effects influencing the process of recording fringe patterns. The applied load causes a distortion of the loading frame. This distortion introduces a rigid body motion of the model. This motion results in the loss of the correlation between the two images, the initial and the final, that are needed to produce a fringe pattern. To minimize a rigid body motion it is necessary to build a very rigid frame. In view of the loads that is necessary to apply to the specimen, this solution is not practical. Three alternative solutions can be followed to take care of this problem, besides reinforcing the frame. The first one is to limit the load to an amount that preserves

the correlation. The second one is to reset the system and to apply additional loading. The third solution is to compensate the rigid body motion. This concept will be analyzed in more details later on. In this series of tests, the loading was limited to the amount that could be applied without causing total decorrelation of the images. The model was subjected to an initial load of about 1600 pounds and the first image was recorded. An additional load was applied until a total of 6 fringes were observed.

The second effect is the turbulence of the air caused by the heat applied to the specimen. It was observed that the pattern motion resulting from the turbulence of the air has an almost periodic character. Hence, the pattern goes through brief stable periods. These periods were used to snap an image.

The tests were carried out at low and at high temperatures. The results of the low temperature tests are summarized in Table III. The strains measured by the strain gage located at the quarter point along the disk diameter are compared with the theoretical and experimental values. The agreement between the three types of values is excellent. It is a well known fact that the experimental values of the strain at the quarter point along the diameter agree with theoretical. Furthermore, the strain distribution at the quarter point is such that the value measured by the strain gage agrees with the value at the centroid of the gage.

The tests at high temperature could not be checked against the high temperature gage because the gage failed. In Fig. 13 and 14 the experimental values are compared with the theoretical values. To obtain this comparison the following procedure was used. The stresses at the quarter point obtained from the theory of the elasticity, together with the experimentally obtained strains were used to obtain the elastic modulus of the material at the corresponding temperature. An independent verification of this procedure was obtained by comparing the obtained elastic moduli with the moduli provided by the manufacturer of the alloy, Fig. 15. The manufacturer's elastic moduli values were obtained from ultrasonic measurements. Since the experimental values correspond to very low stresses, the agreement with the ultrasound measurements is not surprising. Figure 16 shows the fringe pattern corresponding to 900°C.

THIRD SERIES OF TESTS

For the third series of tests the oven was modified, introducing an additional pair of windows to provide vertical illumination. The oven with five windows showed an increased air turbulence when compared to the previous oven configuration. An additional internal window was introduced to reduce the air turbulence.

A second and more rigid loading frame was built. In this series of test it was planned to increase the total load applied to the specimen. The loading mechanism was also modified. The silicon carbide bar used to apply the load developed cracks as a result of the previous tests. It was replaced by a bar of the same Haynes alloy

used in the specimen. The supporting load also cracked and was replaced with a wider stainless steel base protected by a silicon carbide plate.

The third series of test was carried out on another instrumented specimen. Again, besides the thermocouples, low and high temperature gages were fixed on the surface of the specimen.

During the preliminary tests, the upper edge of the disk was damaged and it was necessary to remove a circular sector from both loading areas. The load was applied over a wider area than that resulting from the natural flattening of the contact region.

To increase the total load applied to the specimen, the load step procedure was applied to this series of tests. An initial load of 1.8 kN was initially applied and the load was incremented in steps up to 18 kN. At each load step a new initial image was recorded. The displacements corresponding to each load step were computed. The total displacement was obtained by adding the displacements at each step. The strains corresponding total displacement field were computed. The displacements in the vertical and in the horizontal directions were recorded. Again, the technique to record patterns was to snap a picture each time that the thermal fluctuations of the pattern went through a brief period of stability.

The strains resulting from the optical measurements were compared with the strain gages outputs. Again, the high temperature gages failed. For this reason, the comparisons between the strain gages and the holographically determined values were limited to the low temperature range. The results of these tests are summarized in tables IV and V. These tables give the strain gage values and the holography values for maximum load. The differences between the two measurements are within a 5% difference. Figures 17 and 18 give the comparison of the two sets of readings as a function of the temperature. Figure 19 gives the pattern of the vertical displacements.

The high temperature tests were performed using a different technique to obtain the displacement information. In a previous section we have mentioned the fact that the changes of phase produce by the thermal convective air currents are random in nature. A solution to remove these changes is to compute the phases of a sufficient number of recordings and to average them. Since the changes of phase produced by the loading are stationary in space and time, the average will converge to the stationary value.

The technique of displacement averaging was applied to recordings made at the temperature of 985°C. At this temperature the creep of the metal is pronounced, therefore the stresses were kept low. Forty patterns were snapped at random and the phases of these patterns were computed. The 40 phases were averaged. Figure 20 gives the averaged displacements and Fig. 21 the fringe pattern corresponding to the averaged phase. Figure 22 gives the strains. Figure 23 gives the comparison of the theoretical and the experimental values along the horizontal diameter. It can be seen that the effect of the flattening of the ends of the specimen

does not have a pronounced effect in the strain distribution along the horizontal diameter. The effect of the flattening is pronounced near the region were the load is applied as it can be seen in Fig. 22.

SUMMARY AND CONCLUSIONS

The technology to measure displacements and strains at high temperatures using electronic holography has been successfully developed. The different variables that control the recording of displacements and strains have been individualized. Each one of these variables has been theoretically and experimentally studied. For each one of them, satisfactory compromises have been found between desired results and practical and economical implementation of solutions.

The effect of the light intensity radiated by the surface is reduced by introducing a narrow band pass optical filter, and by improving the surface reflectivity. The improved reflectivity is obtained by applying to the surface a ceramic coating.

The effect of the thermal convective currents is controlled by two separate means. One is to snap the pictures when the thermally generated changes of phase go through brief periods of rest. The other is to average the phases of many recordings. The current version of the instrument has the circuit that compensates the changes of optical phase caused by vibrations, thermal changes in the optical fibers and changes of phase caused by thermal convection currents. This circuit has been successfully checked at room temperature.

The loss of visibility due to the loss of correlation between the initial and final images, is compensated by sequential loading. In the current version of the interferometer, the rigid body motion can be compensated by moving the camera. The compensation has been satisfactorily checked at room temperature.

During the period of the research program, important improvements were introduced in data processing. The addition of a new parallel processor made it possible to implement a 2-D data processing. The 2-D data processing has resulted in an improvement in the quality of the obtained results, as well as in the speed of processing. Currently a full image can be processed in about two minutes.

The application of the interferometer to measure displacements and strains at high temperatures has been carried out through three series of tests. In all three cases accurate quantitative results have been obtained, and these results have been checked by comparison with theory or with other experimental values. These results show beyond doubts that electronic holography can be used as a tool to obtain accurate displacement and strain information at high temperatures.

The development of the program has reached the point where the final phase of the project can be carried out: the construction of a prototype to operate at the NASA-Dryden facilities.

REFERENCES

1. Sciammarella, C.A., "Strains at high temperature by optical techniques," 4th Annual Hostile Environments and High Temperature Measurements, HEHTM, Winsor Locks, CT, SEM, March 1987.
2. Lockberg, O.J., Malmo, J.T. and Slettemoen, G.A., "Interferometric measurement of high temperature objects by speckle pattern interferometry," Applied Optics, 24, (19), 3167, 1985.
3. Malmo, J.T., Lockberg, O.J. and Slettemoen, G.A., "Interferometric testing at very high temperatures by TV holography (ESPI)," Experimental Mechanics, 28, (3), 315, 1988.
4. Sciammarella, C.A, Bhat, G. and Shao, Y., "Measurement of strains at high temperatures by means of a portable holographic moire camera," Proceedings HEHTM, SEM, 21, November 1989.
5. Lant, Ch.T. and Barranger, J.P., "Progress in high temperature speckle shift strain measurement system," Hologram Interferometry and Speckle Metrology, Proceedings SEM, November 5-8, 1990.
6. Kang, J., Wang, F.X. and Liu, O.K., "High temperature moire interferometry for use to 550°C," Hologram Interferometry and Speckle Metrology, Proceedings SEM, November 5-8, 1990.
7. Jones, R. and Wykes, C., Holography and Speckle Interferometry, Cambridge University Press, 1989.
8. Stetson, K.C. and Brohinsky, W.R., "Electro-optical holography and its application to hologram interferometry," Applied Optics, 24, 363, 1985.
9. Sciammarella, C.A., Bhat, G. and Albertazzi Jr., A., "Measurement of strains by means of electro-optics holography," to be published in the proceedings of the SPIE's Optical Engineering Midwest, Chicago, September 21-28, 1990.
10. Sciammarella, C.A. and Ahmadshahi, M.A., "Detection of fringe pattern information using a computer based method," Wieringa, H. (ed.), Experimental Stress Analysis, 15BN90-247-3346-4, Martinus Nijhoff, Dordrecht, 1986.
11. Sciammarella, C.A. and Gilbert, J.A., "Holographic-moire technique to obtain separate patterns for components of displacement", Exp. Mech. 16, (6), 1976.
12. Sciammarella, C.A. and Chawla, S.K., "A lens holographic moire technique to obtain displacement components and derivatives," Exp. Mech., 18, (10), 1978.
13. Gilbert, J.A., Sciammarella, C.A, and Chawla, S.K., "Extension to three-dimensions of a holographic-moire technique to separate patterns corresponding to components of displacement," Exp. Mech., 18, (9), 1978.
14. Sciammarella, C.A., Rastogui, P.K., Jacquot, P. and Natayanan, R., "Holographic-moire in real time," Exp. Mech. 22, (2), 1982.
15. Sciammarella, C.A., "Holographic-moire, an optical tool for the determination of displacements, strains, contours and slopes of surfaces", Optical Eng., 21, (3), 1982.

16. Sciammarella, C.A. and Ahmadshahi, M.A., "A computer based holographic interferometry to analyze 3-D surfaces," IMEKO XI, Instrumentation for the 21st Century, Proceedings of the 11th Triennial Congress, Metrology, Instrument Society of America, 163, 1988.
17. Sciammarella, C.A. and Ahmadshahi, M.A., "Computer aided holographic-moire technique to determine the strains of arbitrary surfaces vibrating in resonant modes," Proceedings of the 1989 SEM Spring Conference on Experimental Mechanics, Boston, 1989, 579.
18. Sciammarella, C.A., Bhat, G. and Albertazzi Jr., A., "Analysis of the sensitivity, an accuracy in the measurement of displacements by means of interferometric fringes," Hologram and Speckle Metroloty, Proceedinsg of SEM, Baltimore, 1990, 310.
19. Fujji, H., Asakura,T. and Shinda, Y., "Measurement of surface roughness properties by using speckle image contrast," J. Opt. Soc. Am., 66, (11), 1976.
20. Fujii, H., Uozomi, J. and Asakura, T., "Computer simulation study of image speckle patterns with relation to the object surface profile," J. Opt. Soc. Am., 66, (11), 1976.

TABLES

Table I
SiC Bar

A $\frac{mW}{cm^2}$	B $\frac{mW}{cm^2}$	C %	D $\frac{\mu W}{cm^2}$	E $\frac{\mu W}{cm^2}$	F %	G $\frac{\mu W}{cm^2}$	J %
.2	1.2	16.6	1.75	.24	13.7	0.08	33.3

Aperture 1/9

Table II
Haynes Alloy

A $\frac{mW}{cm^2}$	B $\frac{mW}{cm^2}$	C %	D $\frac{\mu W}{cm^2}$	E $\frac{\mu W}{cm^2}$	F %	G $\frac{\mu W}{cm^2}$	J %
.22	1.3	16.9	1.75	.58	33.14	.0428	7.3

Aperture 1/7

A Intensity of the laser in the object plane
B Intensity at the furnace window
C A/B in percent
D Intensity (632.8 nm due to temperature computed as shown in [1]
E The same quantity, measured
F E/D in percent
G Intensity of the image plane due to the laser illumination
J G/E in percent

Table III.

Low Temperature Test of the Disk Specimen

Temperature		RT (22.3°C)	200F (93.3°C)	300F (149°C)	400F (205°C)	500F (260°C)
	Theory	94.8	88.06	98.51	100.43	103.11
	Optical	95.6	88.5	97.6	100.0	102.8
ϵx 10^{-6}	Low Temp Gage	91.65	89.5	100.6	101.9	104.56
	High Temp	69.8	84.2	65.5	77.7	90.5
	Theory	-224.8	-224.8	-251.48	-256.4	-263.2
ϵy 10^{-6}	Low Temp Gage	-204.8	-193.1	-217.3	-224.5	-226.6
	High Temp	-207.2	-	-188.3	-99	-188.0
Load (kN)		6.9	6.3	6.9	6.9	6.9

Table IV.

Optical vs. Gage

20.93 kN

Horizontal Illumination and Strains

°C Temp Oven	Gage #4	Optical	% Difference Gage - Optical
23.3 (75)	230$\mu\epsilon$	243$\mu\epsilon$	+5%
93.3 (200)	212$\mu\epsilon$	227$\mu\epsilon$	+6%
149 (300)	205$\mu\epsilon$	221$\mu\epsilon$	+7%
205 (400)	210$\mu\epsilon$'	211$\mu\epsilon$	+0.8%
260 (500)	220$\mu\epsilon$	216$\mu\epsilon$	-1.5%

Table V.
Optical vs. Gage

17.8 kN
Vertical Illumination and Strains

°C (°F) Temp Oven	Gage #3	Optical	% Difference Gage - Optical
23.3 (75)	-529 με	-501με	-5.3%
93.3 (200)	-456με	-477με	+4.6%
149 (300)	-496με	-525με	+5.7%
205 (400)	-512με	-487με	-4.8%
260 (500)	-499με	-507με	+1.6%

FIGURES

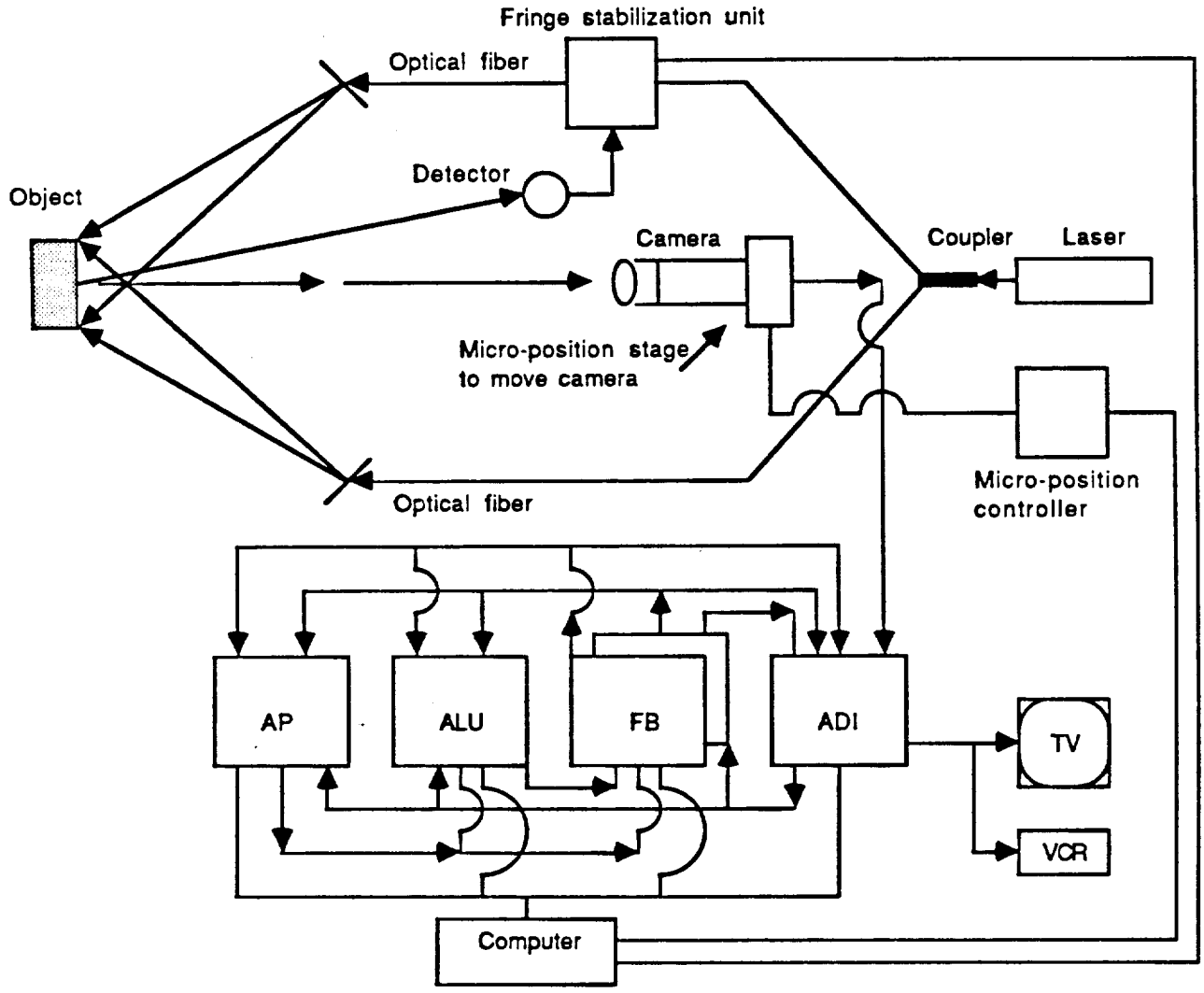

ADI - Alalog to digital interface FB - Frame buffer ALU - Arithmetic and logic unit
AP - Array Processor

Fig. 1 Schematic representation of the electro-optical system used to measure strains at high temperature

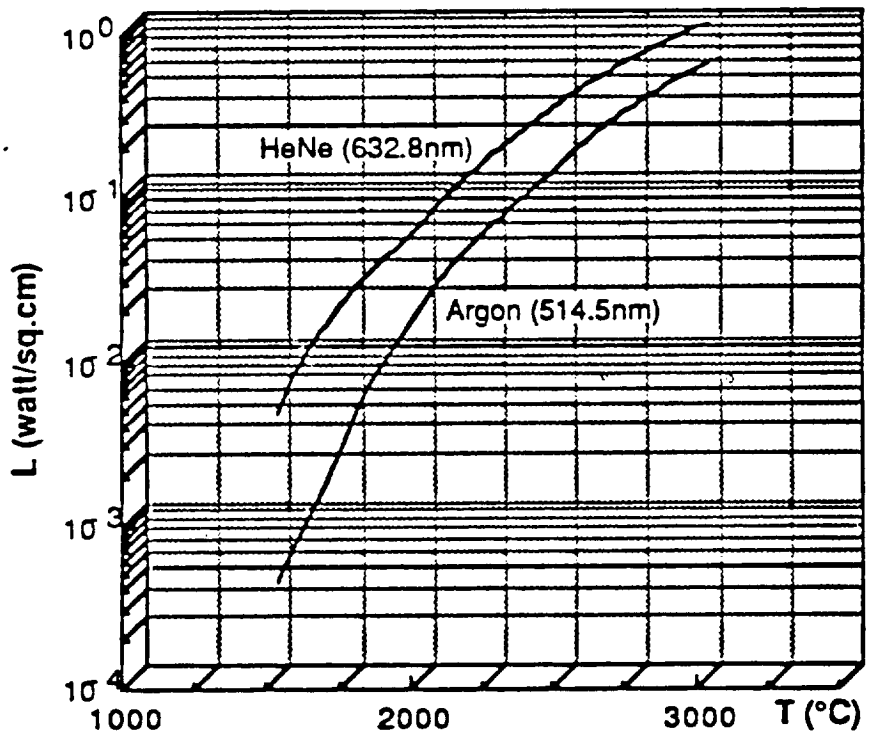

Fig. 2 Background radiation energy for the black body (emmisivity $\epsilon = 1$) as a function of the temperature

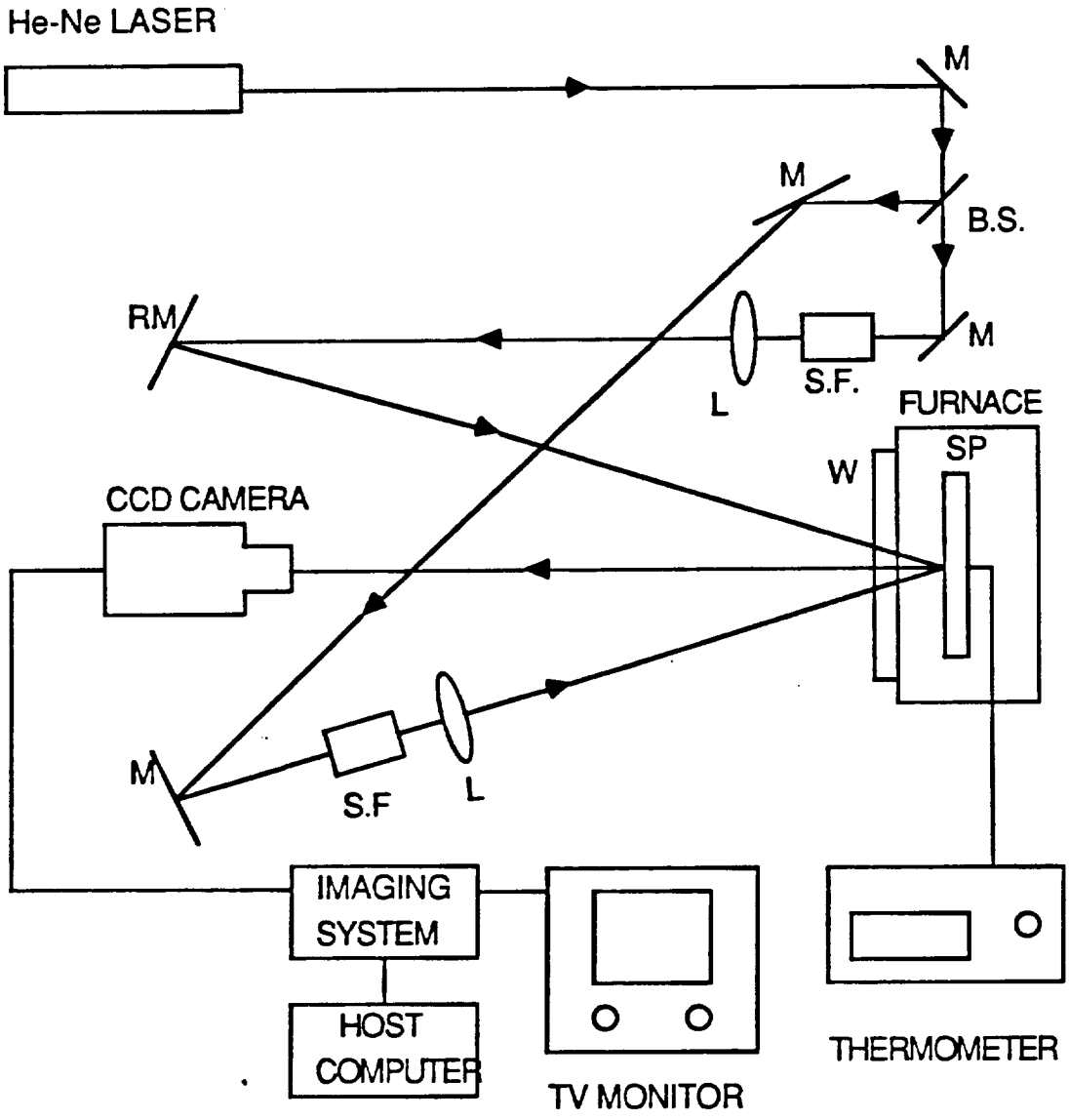

M: MIRROR R.M. : ROTATABLE MIRROR SP : SPECIMEN

L: COLLIMATING LENS S.F. : SPATIAL FILTER W: WINDOW

B.S. : BEAM SPLITTER

Fig. 3 Optical setup

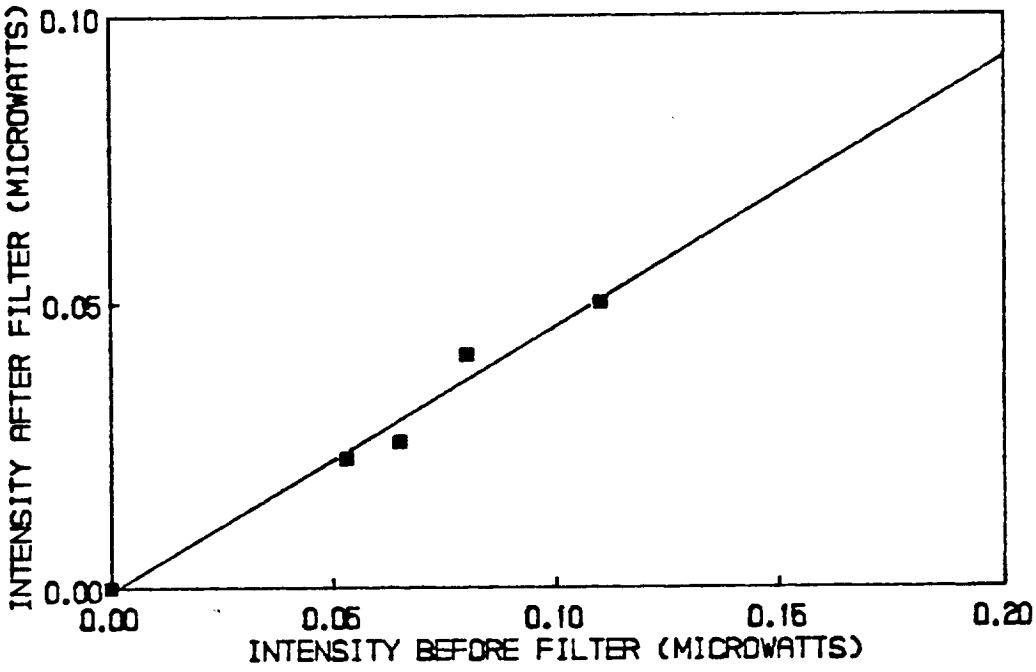

Fig. 4 Transmission function of the filter

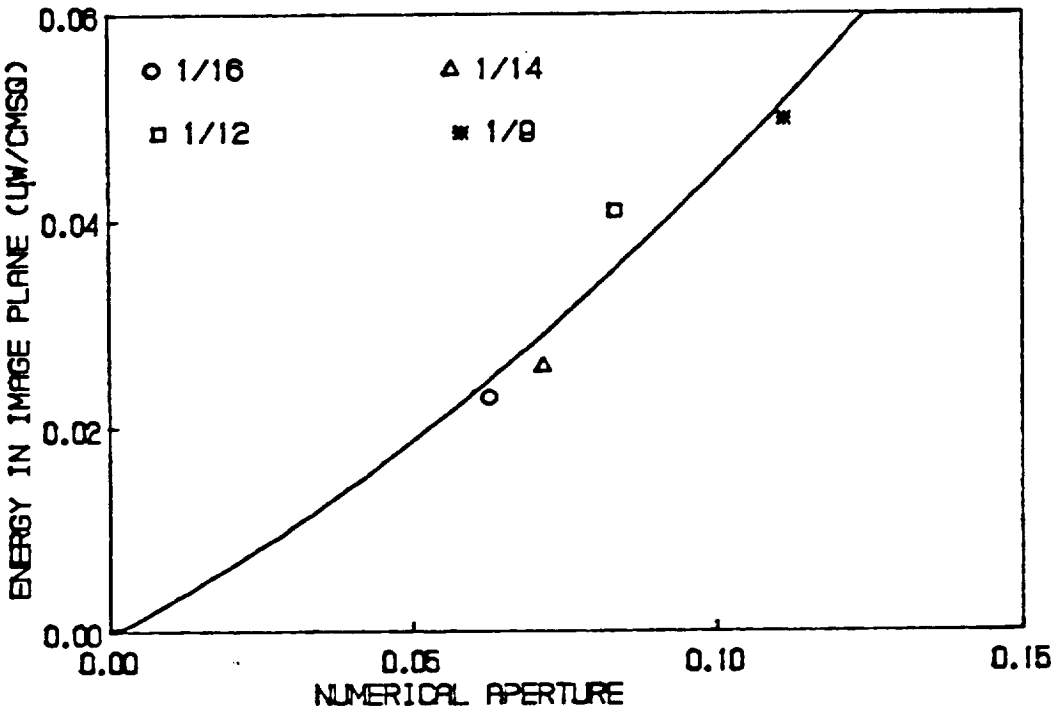

Fig. 5 Energy in image plane vs. numerical aperture of lens

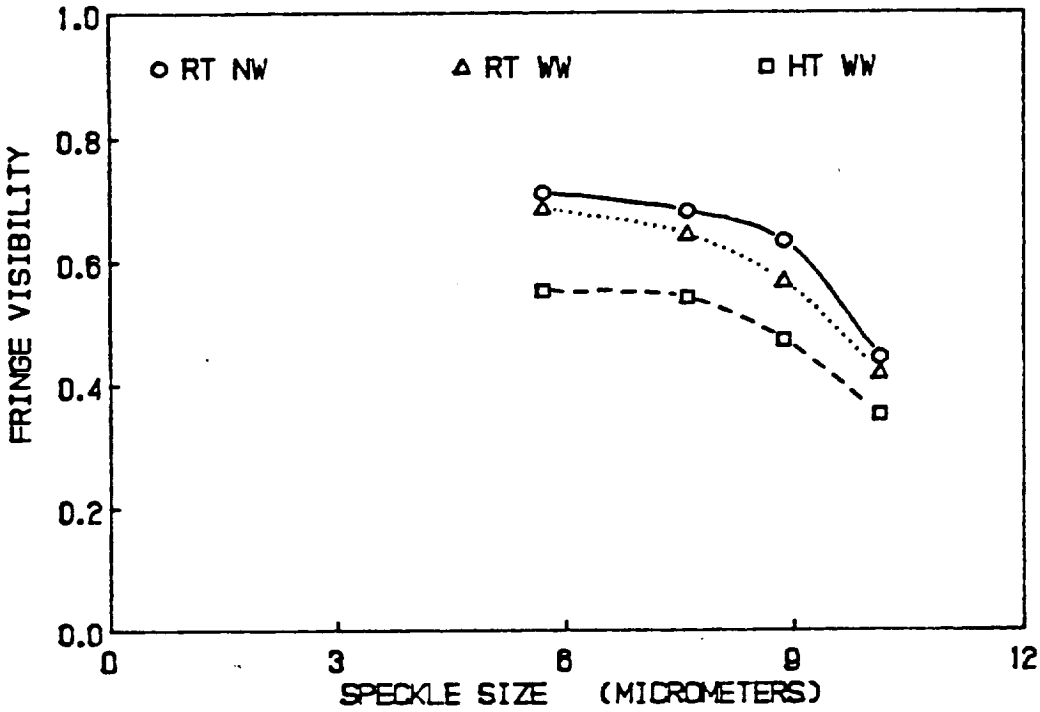

Fig. 6 Fringe visibility vs. speckle size (SiC) specimen

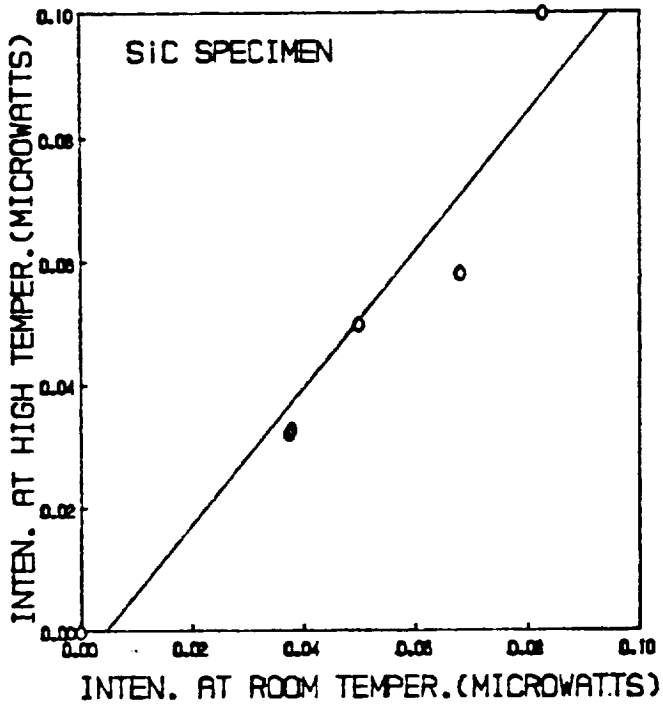

Fig. 7 Intensity in image plane at high temperature vs. intensity in the image plane at room temperature

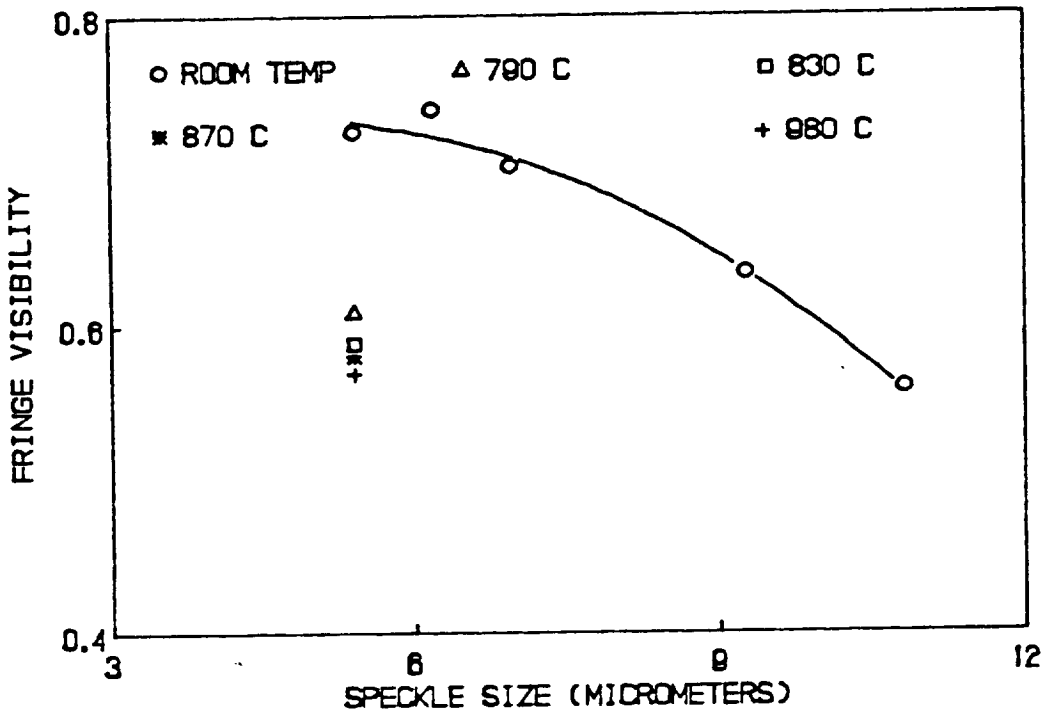

Fig. 8 Fringe visibility vs. speckle size (Haynes Alloy)

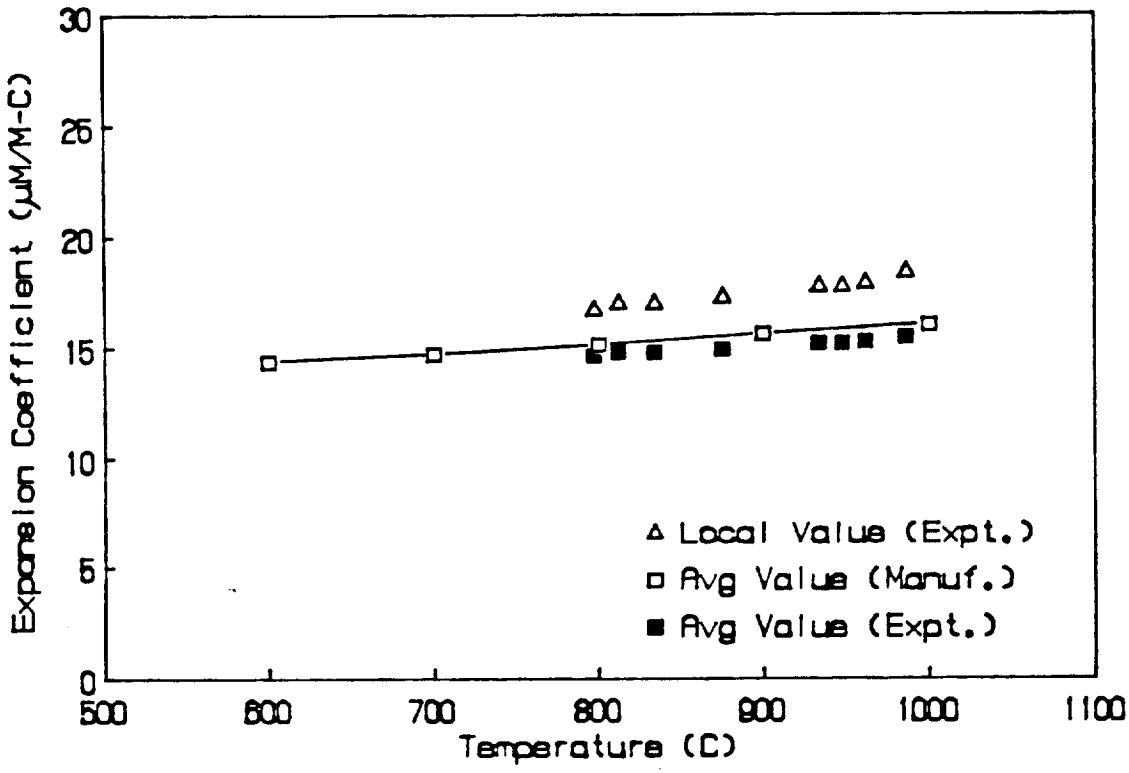

Fig. 9 Coefficient of expansion of the Haynes 230 Alloy

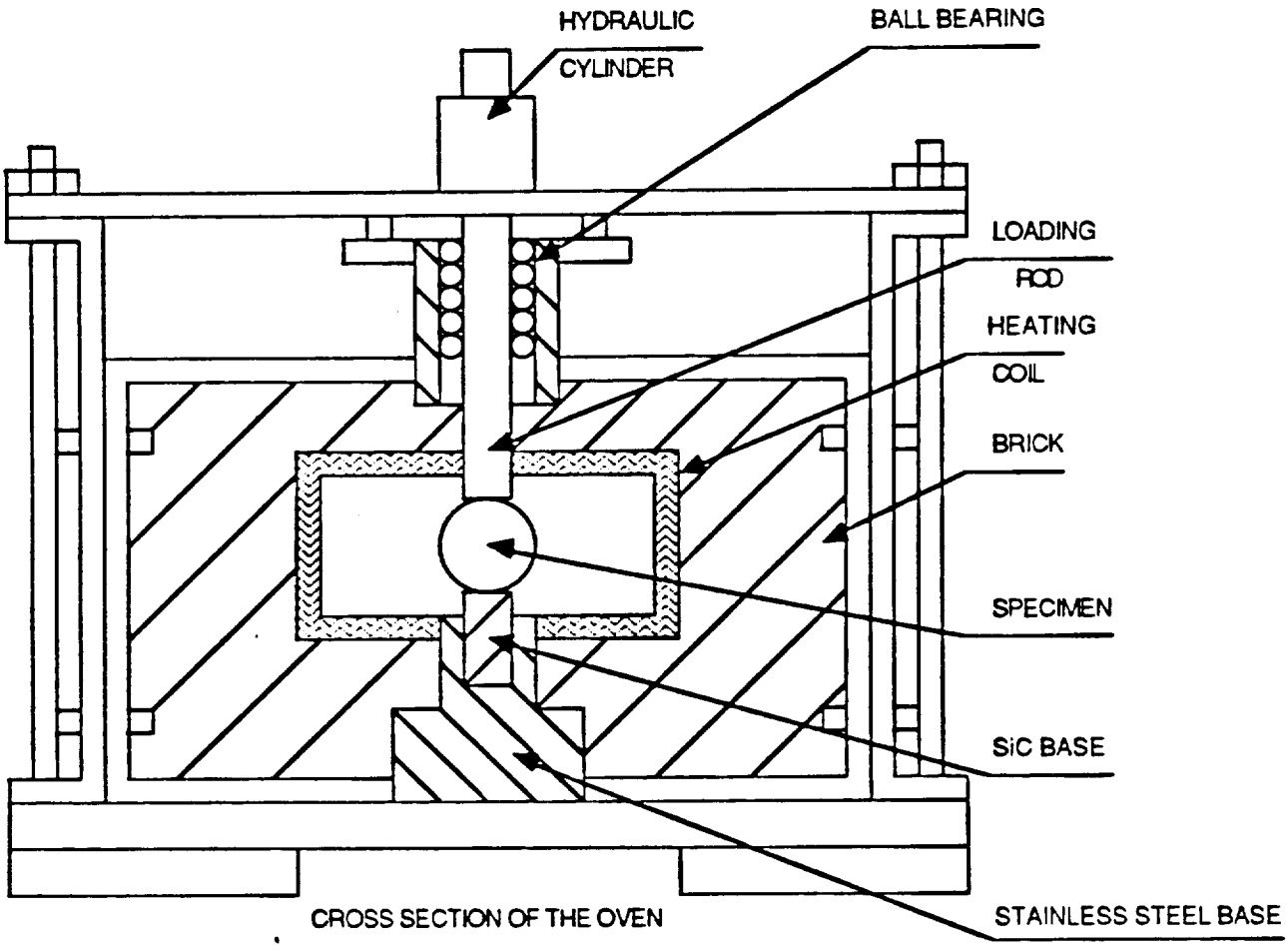

Fig. 10 High temperature oven built to test specimens at 1000°C

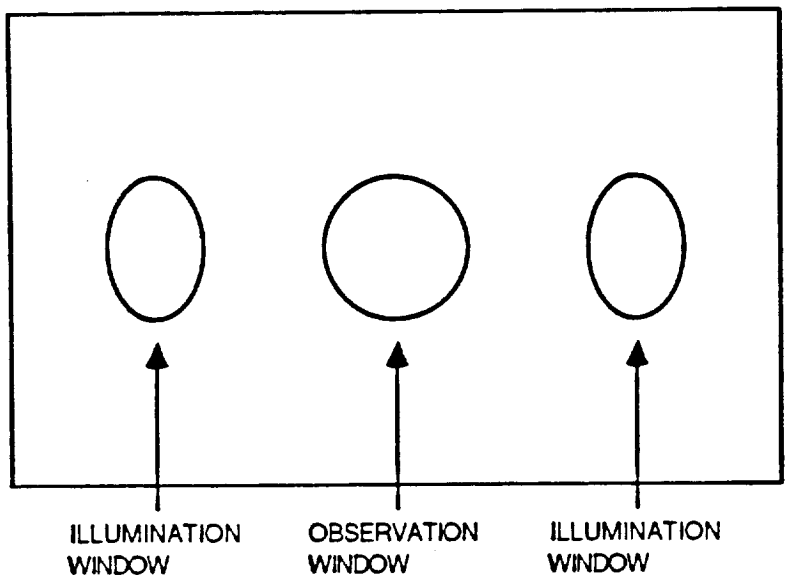

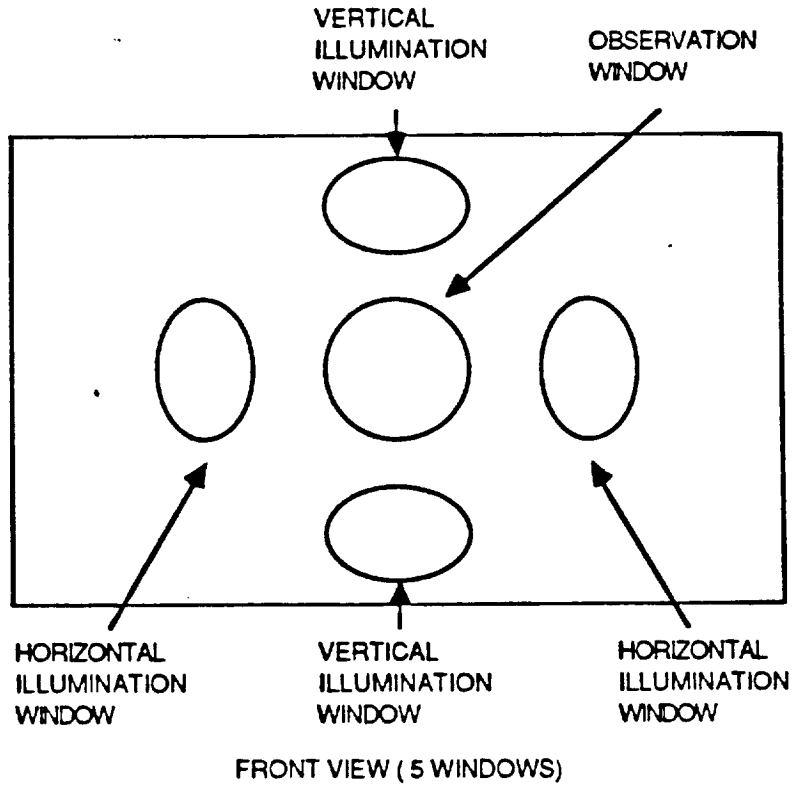

Fig. 11 Windows configurations of the oven built to test specimens at 1000°C

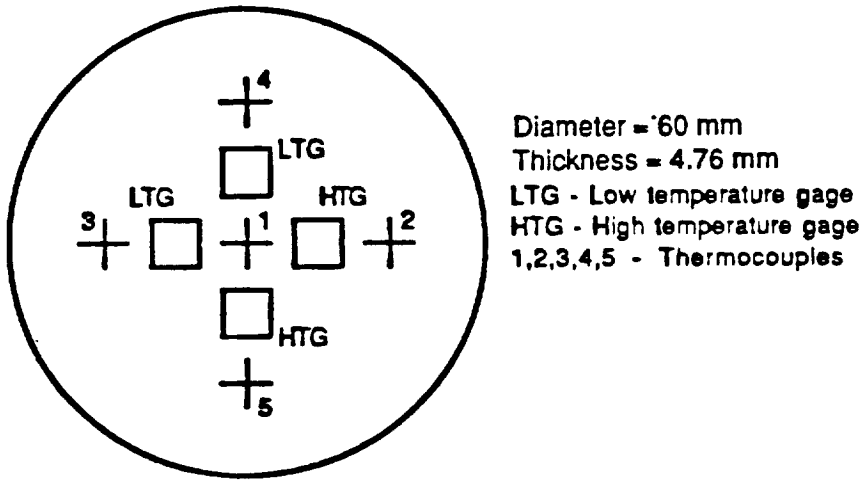

Fig. 12 Location of thermocouples and strain gages in the disk specimens used in the series 2 and series 3 tests

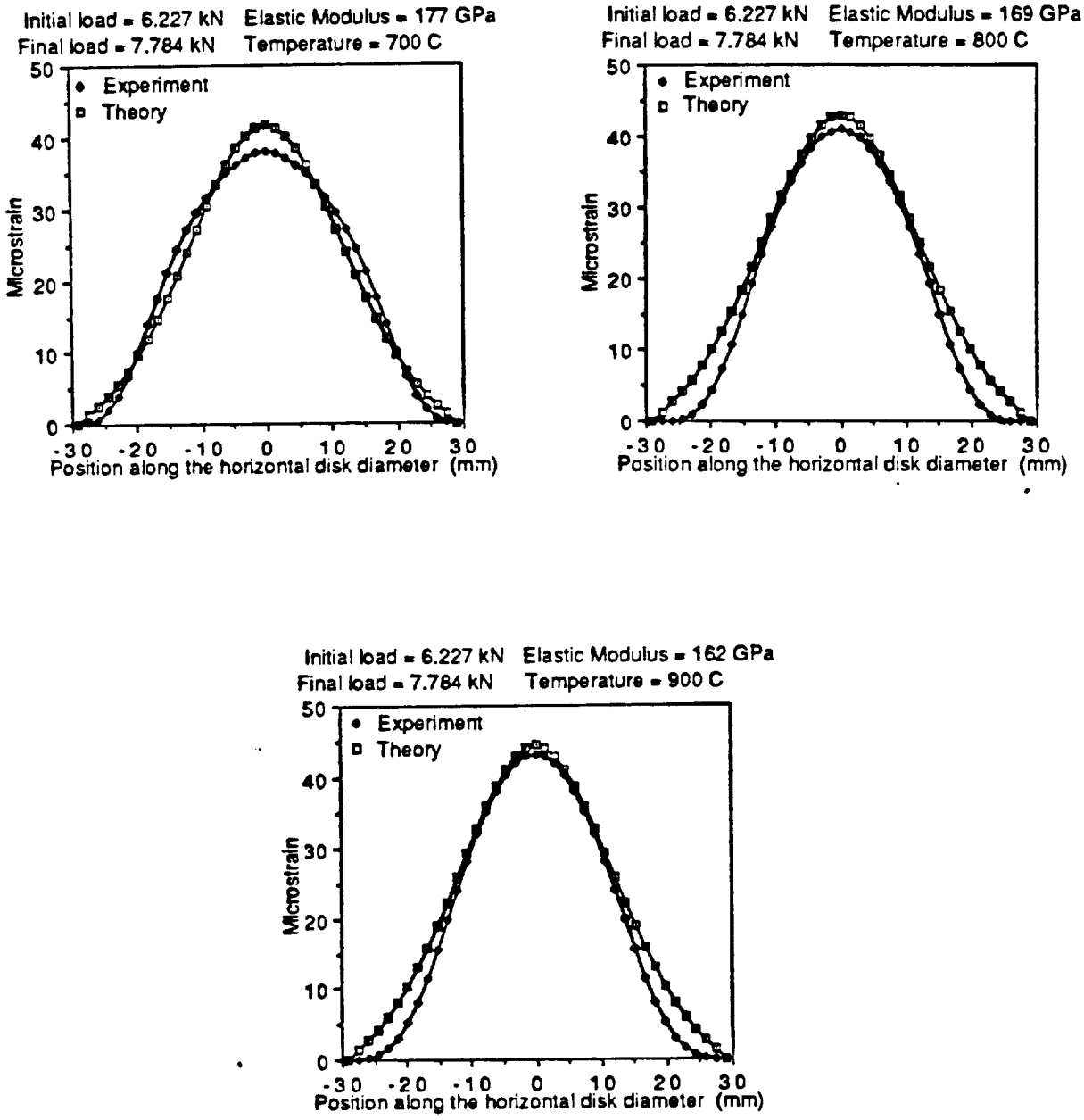

Fig. 13 Comparison of the elastic solution with the electro-optical holographic-moire results

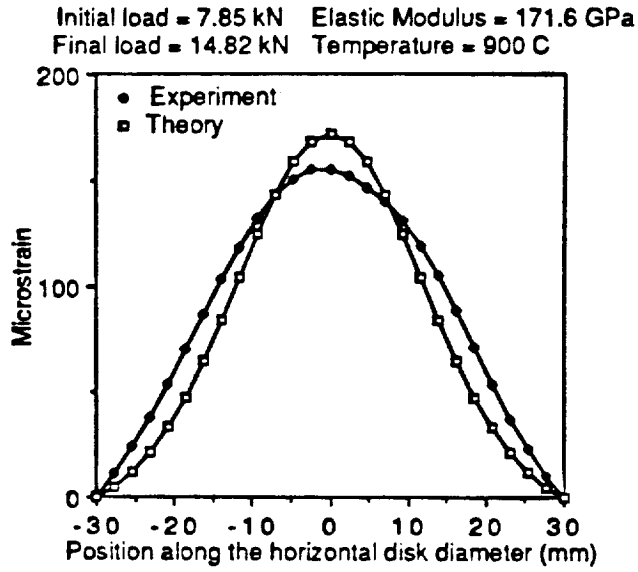

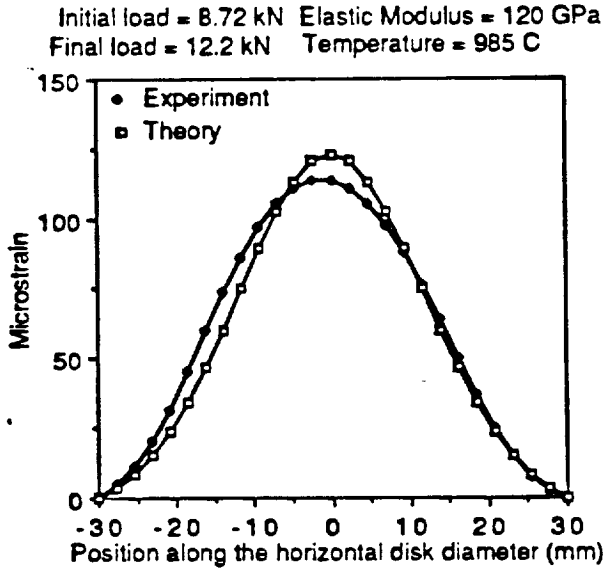

Fig. 14 Comparison of the elastic solution with the electro-optical holographic-moire results, strains along the horizontal axis

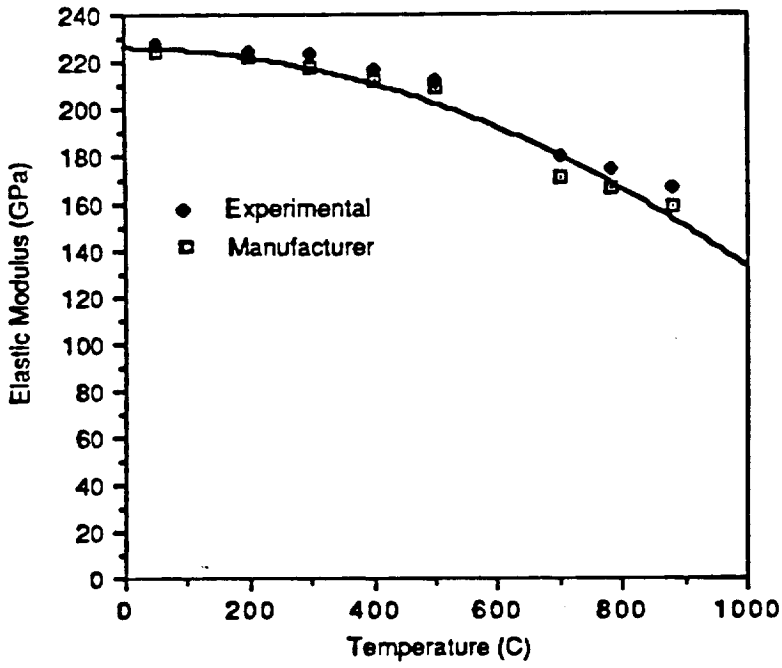

Fig. 15 Comparion of the Young's modulus computed from the disk tests with the manufacturer provided values (Haynes Alloy No. 25)

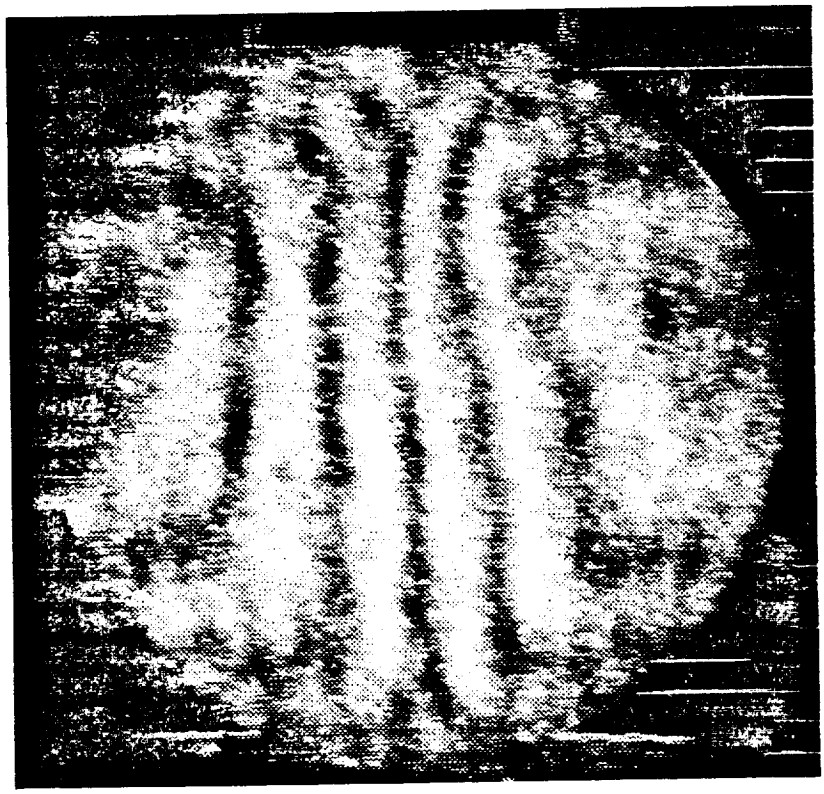

Fig. 16 Fringe patterns corresponding to 900°C, u-displacements

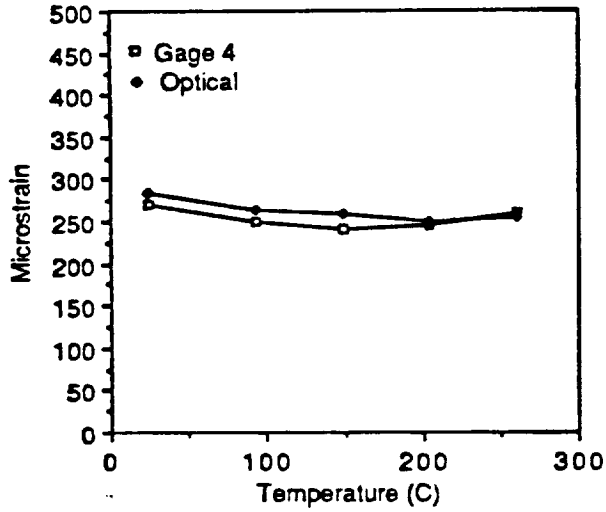

Fig. 17 Comparison of the strain gage and optically measured strains as a function of the temperature horizontal diameter, gage 4 (horizontal direction)

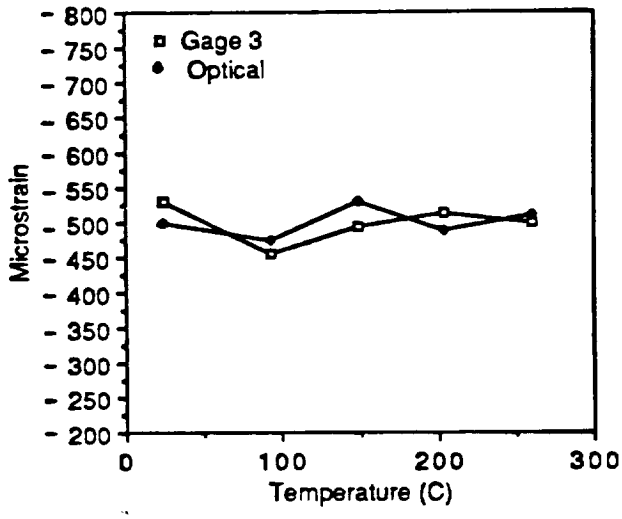

Fig. 18 Comparison of the strain gage and the optically measured strains, horizontal diameter gage 3 (vertical direction)

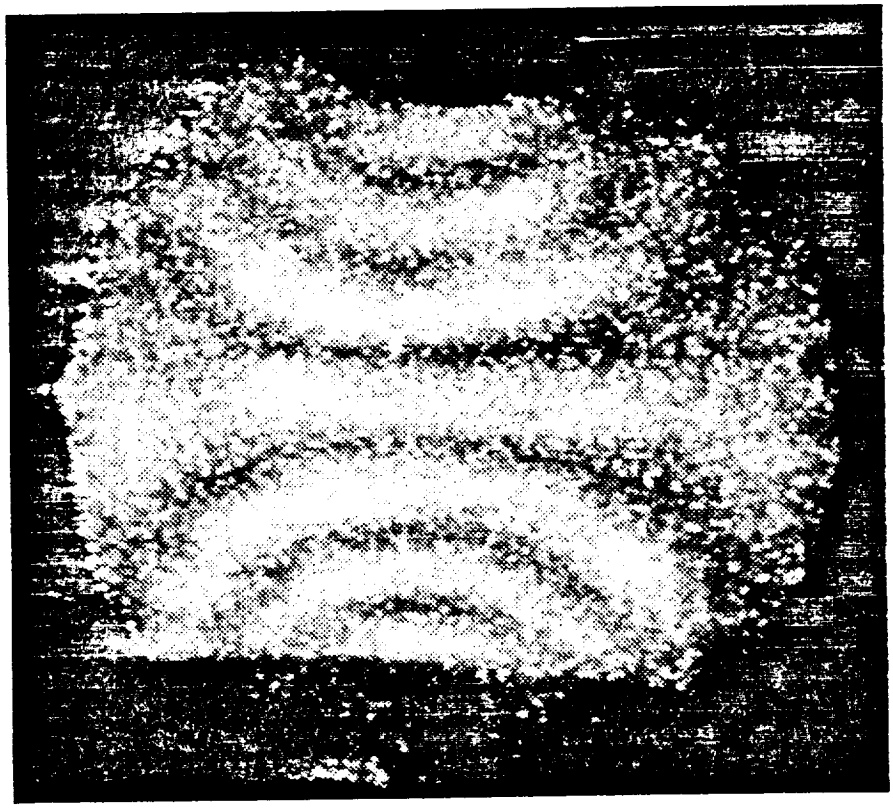

Fig. 19 Pattern corresponding to the vertical displacements, 900°C

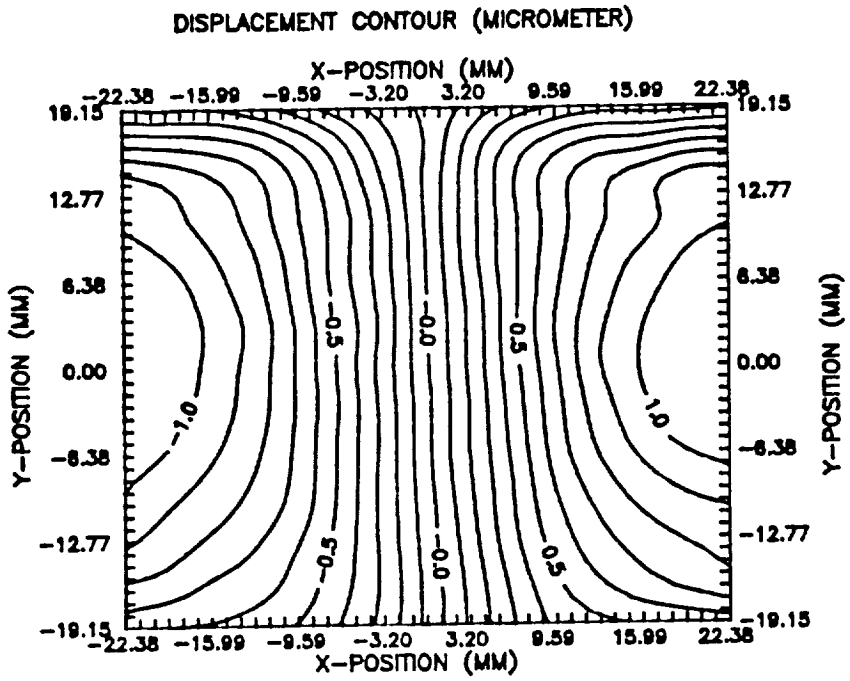

Fig. 20 Displacement contours corresponding to the average of 40 patterns

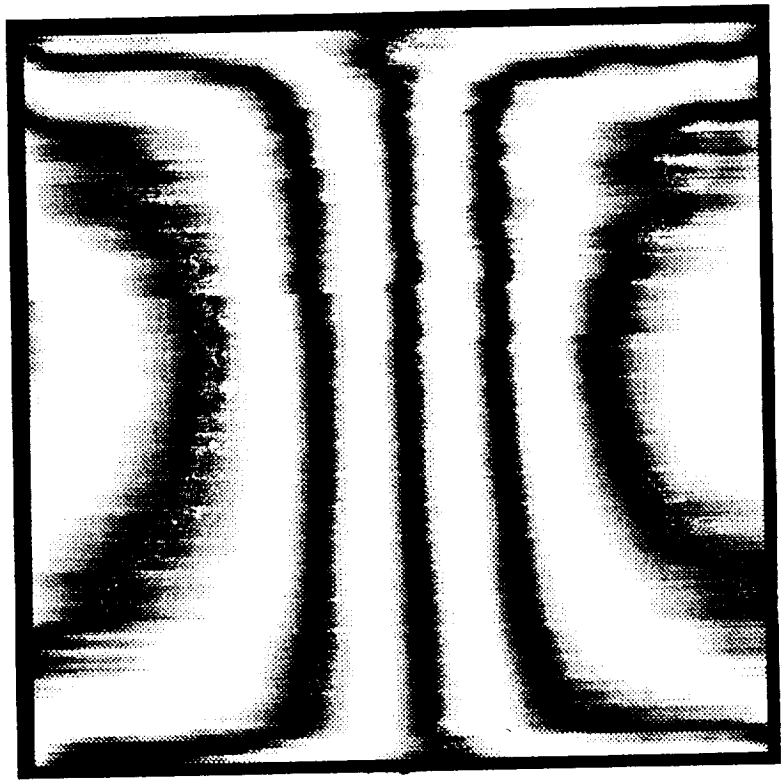

Fig. 21 Pattern resulting from the phase averaging of 40 patterns recorded at 985°C

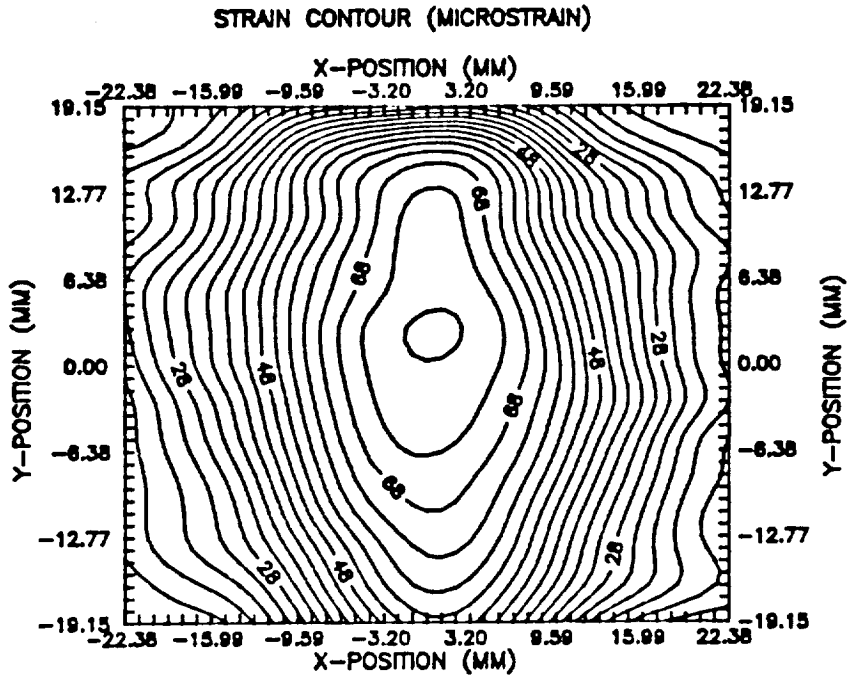

Fig. 22 Strain contours corresponding to the pattern of Fig. 21

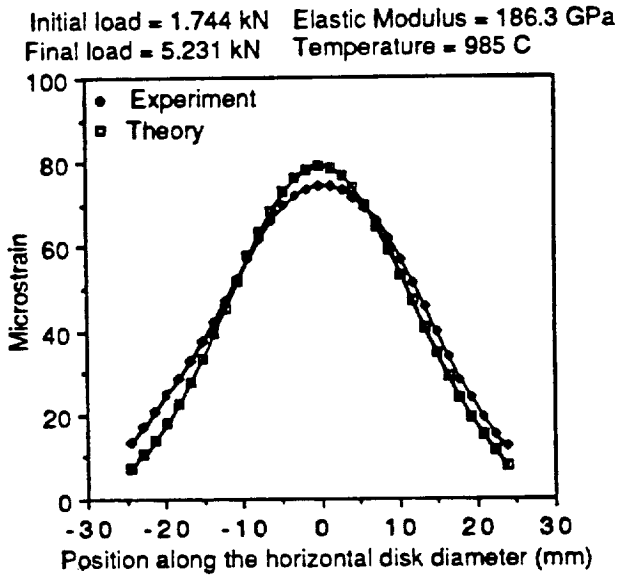

Fig. 23 Comparison of theoretical and experimental results along the horizontal diameter (values correspond to Fig. 22). Load 5.23 kN, T 985°C

APPENDIX

MEASUREMENT OF STRAINS AT HIGH TEMPERATURES BY MEANS OF A PORTABLE HOLOGRAPHIC MOIRE CAMERA

C.A. Sciammarella, G. Bhat and Y. Shao
Illinois Institute of Technology
Department of Mechanical and Aerospace Engineering
Chicago, IL 60616

ABSTRACT

Electronic holographic moire is utilized to measure strains at temperatures up to 1000°C. A cw laser operating at 50 mW and at the wavelength of 632.8 nm is used to illuminate the objects under study. The main variables influencing the fringe patterns visibility are discussed and measurements are performed to obtain the values of these variables in the performed experiments. The coefficient of expansion of an alloy is measured at temperatures ranging from 797°C to 986°C. Excellent agreement is found between the measured values and those provided by the manufacturer.

Proceedings of SEM, Hostile Environments and High Temperature Measurements, Nov. 6-8, 1989, Kansas City, Missouri.

MEASUERMENT OF STRAINS AT HIGH TEMPERATURES BY MEANS OF ELECTRO-OPTICS HOLOGRAPHY

Cesar A. Sciammarella, G. Bhat and Jeffrey Vaitekunas
Illinois Institute of Technology
Department of Mechanical and Aerospace Engineering
Chicago, IL 60616

ABSTRACT

Electro-optics holographic-moire interferometry is used to measure strains at temperatures up to 1000°C. A description of the instrumentation developed to carry out the measurements is given. The data processing technique is also explained. Main problems encountered in recording patterns at high temperatures are analyzed and possible solutions are outlined. Optical results are compared with strain gage values obtained with instrumented specimens and with theoretical results. Very good agreement is found between optical, strain gage and theoretical results.

Proceedings of the 1991 SEM Spring Conference on Experimental Mechanics, June 10-13, Milwaukee, Wisconsin.

APPLICATION OF ELECTRO-OPTICAL HOLOGRAPHY TO THE MEASUREMENT OF STRAINS AT HIGH TEMPERATURES

Cesar A. Sciammarella, G. Bhat and Donald R. Matthys
Illinois Institute of Technology
Department of Mechanical and Aerospace Engineering
Chicago, IL 60616

ABSTRACT

The measurement of strains at temperatures of the order of 1000°C has become a very important field of research. Technological advances in areas such as the analysis of high speed aircraft structures and high efficiency thermal engines require operational temperatures of this order of magnitude. Current techniques for the measurement of strains such as electrical strain gages, are at the limit of their useful range and new methods need to be developed. Optical techniques are very attractive in this type of application because of their noncontacting nature. Holography is of particular interest because a minimal preparation of the surfaces is required. Opto-electronics holography is specially suited for this type of application, from the point of view of industrial use. There are a number of technical problems that is necessary to overcome to measure strains using holographic interferometry at high temperatures. This paper discuss and gives solutions to some of these problems. A specimen instrumented with high temperature strains gages is used to compare the results of both technologies.

To be presented at the SPIE International Symposium on Optical Applied Science and Engineering, July 19-24, 1992, San Diego, California.

PUBLICATIONS

[1] Sciammarella, C.A., Bhat, G. and Shao, Y., "Measurement Of Strains At High Temperatures by Means of a Portable Holographic Moire Camera," SEM, Hostile Environments and High Temperature Measurements, Nov. 6-8, 1989, Kansas City, Missouri.

[2] Sciammarella, C.A., Bhat, G. and Vaitekunas, J., "Measurement of Strains at High Temperatures by Means of Electro-Optics Holography," Proceedings of the 1991 SEM Spring Conf. on Experimental Mechanics, June 10-13, 1991, Milwaukee, Wisconsin.

[3] Sciammarella, C.A., Bhat, G. and Matthys, D., "Application of Electro-Optical Holography to the Measurement of Strains at High Temperatures," to be presented at the SPIE International Symposium on Optical Applied Science and Engineering, July 19-24, 1992, San Diego, California.